Numerical survey of the tunable condensate shape and scaling laws in pair-factorized steady states

Numerical survey of the tunable condensate shape and scaling laws in pair-factorized steady states

Eugen Ehrenpreis, Hannes Nagel and Wolfhard Janke

Institut für Theoretische Physik, Universität Leipzig, Postfach 100 920,
D-04009 Leipzig, Germany

E-mail: Eugen.Ehrenpreis@itp.uni-leipzig.de, Hannes.Nagel@itp.uni-leipzig.de and
Wolfhard.Janke@itp.uni-leipzig.de

Abstract

We numerically survey predictions on the shapes and scaling laws of particle
condensates that emerge as a result of spontaneous symmetry breaking in pair-
factorized steady states of a stochastic transport process. The specific model
consists of indistinguishable particles that stochastically hop between sites
controlled by a tunable potential. We identify the different condensate shapes
within their respective parameter regimes as well as determine precisely the
condensate width scaling.

(Some figures may appear in colour only in the online journal)

1. Introduction

In stochastic mass transport processes, one is generally concerned with the dynamics of
abstract, usually indistinguishable particles. Well known models include the totally asymmetric
exclusion process [1, 2] where the unidirectional free movement of particles is hindered by
other particles, and the more generic zero-range process (ZRP) [3] that only models zero-
ranged interactions of particles. Depending on the situation and given type of dynamics these
particles may represent actual molecules on the microscopic scale, mesoscopic objects like
intracellular motor proteins [4] or even macroscopic bodies such as people or cars in traffic
systems [5]. Interesting effects such as phase transitions in the one-dimensional system and
real-space condensation of particles can already be seen in the ZRP, despite the absence

of ranged interactions [6–9]. In this paper we will consider a generalized transport process including short-ranged interactions which allows for a pair-factorized steady state [10]. For a specific type of interactions proposed by Wacław *et al* [11], this model features a spatially extended condensate that can assume several distinguished shapes. That is, by parametrization the condensate can be tuned to a single-site peak, rectangular or smooth parabolic envelope shape. Here we will consider and validate predictions on the scaling of the condensate width as well as its shape made in [11, 12].

The rest of the paper is organized as follows. In the next section we will introduce the considered stochastic transport model and summarize the derivation of the predictions. The methods needed to simulate the model and measure its properties will be discussed in the third section followed by a discussion of our results in the fourth section. The paper closes with our conclusions in the fifth section.

2. Model

Consider M indistinguishable particles on a one-dimensional, periodic lattice with N sites. Any site i can be occupied by any number of particles $m_i \geqslant 0$. We only consider closed systems, that is, the number of particles is conserved, $M = \sum_{i=0}^{N} m_i$, with an overall density $\rho = M/N$. The dynamics is defined as a Markovian stochastic process: At any time step, a particle may leave from a randomly selected site and move to either of its neighbours. The specific dynamics is largely controlled by the hopping rate $u(m_i | m_{i-1}, m_{i+1})$, which determines whether a particle actually performs a hop. The fact, that it depends only on the occupation numbers of the selected site and those of its direct neighbours, reflects the short interaction range of particles and sites.

The model can easily be tuned from symmetric to totally asymmetric dynamics by introducing a probability r, that is used to decide whether a particle hops to the right or left neighbour. Even though this allows tuning the process from equilibrium ($r = 1/2$) to non-equilibrium ($r \neq 1/2$) dynamics, the stationary state remains unaffected.

2.1. Definitions

Such a model was proposed by Evans *et al* [10] as an extension of the well known ZRP and therefore inherits several of its properties: The model features a stationary state that may contain a particle condensate. The steady state probabilities $P(\vec{m})$ factorize over symmetric non-negative weight functions $g(m, n)$ of *pairs* of sites

$$P(\vec{m}) = P(m_1, \ldots, m_N) = \frac{1}{Z} \prod_{i=1}^{N} g(m_i, m_{i+1}) \tag{1}$$

for $\sum m_i = M$ kept constant, with the partition function $Z = \sum_{\{\vec{m}\}} P(\vec{m})$ and the configuration space $\{\vec{m}\}$. In contrast, for the ZRP, the state probabilities factorize over *single-site* weight functions.

If the weight function $g(m_i, m_i + 1)$ falls off faster than any power law, it has been shown that there exists a critical density ρ_c, above which translational symmetry is broken and a particle condensate emerges [10–12]. That is, in the steady state the bulk system can only hold a limited number of particles given by ρ_c and any further added particle increases only the condensate mass $M_c = M - \rho_c N = (\rho - \rho_c)N$.

The hopping rate that leads to the steady state (1) is easily determined with the weight function $g(m, n)$ as

$$u(m_i|m_{i-1}, m_{i+1}) = \frac{g(m_i - 1, m_{i-1})}{g(m_i, m_{i-1})} \frac{g(m_i - 1, m_{i+1})}{g(m_i, m_{i+1})} \qquad (2)$$

by resolving the balance condition in the steady state. In the case of symmetric hopping, detailed balance is fulfilled.

An interesting way to construct such weights is to simplify and separate

$$g(m, n) = \sqrt{p(m)p(n)}K(|m - n|), \qquad (3)$$

i.e., to factorize $g(m, n)$ into a zero-range part $p(m)$ and a short-range interaction part $K(|m-n|)$ that depends on the difference of nearest-neighbour occupation numbers. The term *zero-range* interaction refers to the fact that it allows a particle on a given site to interact with particles on that site only. In contrast, *short-range* interactions act between particles of different sites. For example, the zero-range process [3] with the hopping rate $u(m) = 1 + b/m$ is easily implemented using the weight function $p(m) = \prod_{n=1}^{m} = \frac{1}{u(n)}$, $p(0) = 1$, with $K(x) = 1$ as there is no short-range interaction involved.

In the original model by Evans *et al* [10] governed by the weights

$$K(x) = \exp(-J|x|), \quad p(m) = \exp(U_0\delta_{m,0}), \qquad (4)$$

the condensate has a characteristic smooth parabolic shape. Under the conditions that $K(x)$ falls off faster than any power law and $p(m) = $ const for some $m > m_{\max}$, the exact envelope shape can be calculated as well as its fluctuations and the condensate width scaling behaviour $W \propto \sqrt{M_c}$ [12]. The factorization (3) of $g(m, n)$ also makes it easier to understand the physical picture of condensation involved. The zero-range potential $p(m)$ gives a penalty to increasing occupation numbers, much like a potential energy term, while the short-range interaction $K(x)$ tends to reduce the difference in occupation numbers of neighbouring sites, acting like a surface energy. It is then the respective relative importance of these terms that governs the properties of the emerging condensate.

Wacław *et al* [11] then suggested a family of weights

$$K(x) \sim e^{-a|x|^\beta}, \quad p(m) \sim e^{-bm^\gamma} \qquad (5)$$

that allows one to deliberately violate the asymptotic condition on $p(m)$ for large m by choice of parameters. This produces regimes featuring qualitatively different condensation properties, and most notably may be used to tune the condensates envelope shape as well as the scaling behaviour of its width with system size [11, 12]. In [12] these regimes and properties are derived in the large-volume limit of the model. It is the subject of this work to check these predictions by means of numerical simulations at finite volumes and scaling analyses. In the next subsection we will therefore shortly summarize the derivation of the interesting new properties.

2.2. Theoretical predictions

The proposed model is fully defined by equations (1), (3), and (5). The parameters β, γ give the respective growth behaviour of the short-range and zero-range interaction strengths and are expected to have the most influence on condensation properties. The factors a, b allow to tune the relative strengths of the interactions but do not change the qualitative behaviour of the system as we will see later. In this paper we will therefore use $a = b = 1$.

First, the condition $\gamma \leqslant 1$ is derived to observe condensation at all. Next, the steady state weight equation (1) can be thought to factor into one part accounting for the statistical weight

of the condensate and one for that of the rest of the system. Then, a comparison of the weight of a single-site condensate P_1 and that of a condensate occupying two or more sites P_n shows that for $\beta > \gamma$ the weight P_n grows faster than P_1, so that an extended condensate can be expected in the large system-size limit.

In the case of the extended condensate a similar approach is used to predict some of its properties. Under the assumption, that the contribution of fluctuation of occupation numbers is small compared to the contribution from the condensate itself, the weight of a condensate extended over W sites is given as [12]

$$\ln P(W) \approx Wc + \sum_i \ln K(\langle m_{i+1} - m_i \rangle) + \sum_i \ln p(\langle m_i \rangle), \tag{6}$$

where for simplicity $c = s - \ln \lambda_{\max}$ is treated as a positive constant to approximate the partition function, with an entropic term s that corresponds to fluctuations of the occupation numbers and the largest eigenvalue $\lambda_{\max}$ of the associated transfer matrix. The expectation values $\langle m_i \rangle$ correspond to values $Hh(2i/W - 1)$ where $h(\xi)$ with $\xi = 2i/W - 1$ is the rescaled envelope shape of a condensate with height $H = M_c/W$ and width W. Now, for the expectation of occupation number differences $\langle m_{i+1} - m_i \rangle$ a distinction into two cases is proposed to allow simplifications. Either, the envelope shape $h(\xi)$ is smooth or it is of rectangular shape. In the first case the expectation of the difference can be written using the derivative of the shape $h'(\xi)$ and the expectation reads $(2M_c/W^2)h'(\xi)$. In the second suggested case, all differences are zero except at the condensate boundaries and the sum reduces to a single term. Then in both cases, the sums can be written as integrals using the rescaled shapes resulting in

$$\ln P_{\text{smooth}}(W) \approx W \left[c + \int_0^1 d\xi \ln K \left(\frac{2M_c}{W^2} h'(\xi) \right) + \int_0^1 d\xi \ln p(Hh(\xi)) \right], \tag{7}$$

$$\ln P_{\text{rect}}(W) \approx Wc + 2 \ln K \left(h(1) \frac{M_c}{W} \right) + W \int_0^1 d\xi \ln p(Hh(\xi)). \tag{8}$$

The sums decouple into a prefactor and a constant integral term, which does not depend on the condensate width. The prefactors however are used to determine the growth of the different condensate weights depending on their respective widths and masses:

$$\ln P_{\text{smooth}}(W) \approx W \left[c - a \left(\frac{2M_c}{W^2} \right)^\beta \int_0^1 d\xi \, |h'(\xi)|^\beta - b \left(\frac{M_c}{W} \right)^\gamma \int_0^1 d\xi \, |h(\xi)|^\gamma \right], \tag{9}$$

$$\ln P_{\text{rect}}(W) \approx Wc - a \left(\frac{M_c}{W} \right)^\beta 2|h(1)|^\beta - bW \left(\frac{M_c}{W} \right)^\gamma \int_0^1 d\xi \, |h(\xi)|^\gamma. \tag{10}$$

Finally, the condensate weights are estimated[1] by finding their maximal value with respect to the condensate width (with constant mass) which also gives the scaling laws for the condensate width

$$\ln P_{\text{smooth}}(W) \sim -M_c^{(\gamma\beta+\beta-\gamma)/(2\beta-\gamma)}, \quad W \sim M_c^{(\beta-\gamma)/(2\beta-\gamma)} \quad \text{for} \quad \beta > \tfrac{1}{2}, \quad \text{and} \tag{11}$$

$$\ln P_{\text{rect}}(W) \sim -M_c^{\beta/(\beta-\gamma+1)}, \quad W \sim M_c^{(\beta-\gamma)/(\beta-\gamma+1)} \quad \text{for} \quad \beta > 0 \tag{12}$$

in the smooth and rectangular case, respectively. For $0 < \beta < 1/2$, no solution exists for smooth condensates. Finally these weights are compared to find $\ln P_{\text{rect}}(W) > \ln P_{\text{smooth}}$ for

---

[1] During the estimation of the maximal weight for the given condensate type additional constraints are found [12], where no solution exists, narrowing down the number of cases to look at.
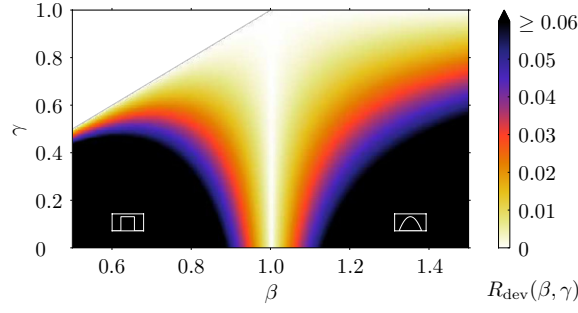
Figure 1. Comparing the scaling behaviours of the most likely rectangular and smooth condensate shapes using the relative deviation (13), over a region in β-γ-parameter space. Larger deviations R_{dev} (cut off at 0.06) mean that (in the thermodynamic limit) the probabilities are different, and lower ones that they are close.
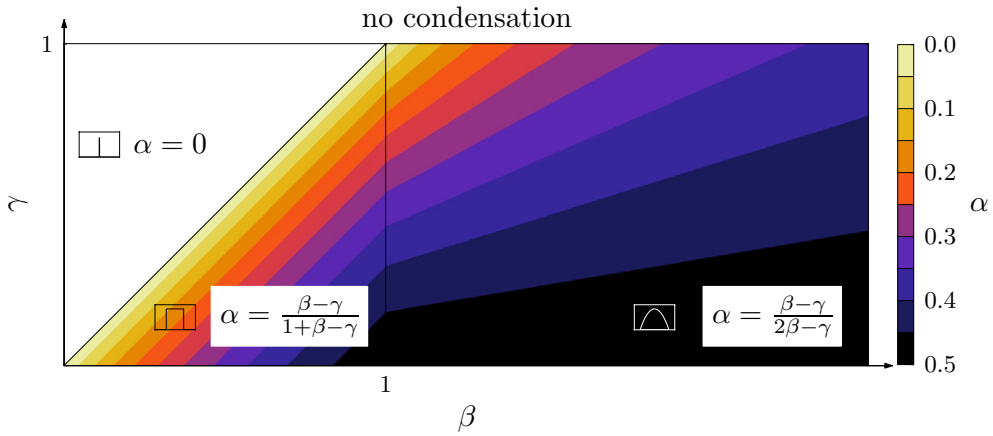

Figure 2. The width-scaling exponent α in $W \propto M_{\text{c}}^{\alpha}$ for different parametrizations β and γ, cf equation (14). The three regions of different scaling behaviour mark the distinctive phases. For $\gamma \geqslant 1$ there is no condensation. This figure is plotted from figure 5 in [12].

$1/2 < \beta < 1$, showing that the rectangular shape is the stable one in this regime. In figure 1 we plot the (M_{c}-independent) relative deviation

$$R_{\text{dev}}(\beta, \gamma) = \frac{\log(-\log P_{\text{smooth}}) - \log(-\log P_{\text{rect}})}{\log(-\log P_{\text{rect}})} \tag{13}$$

to give an impression of the regime boundary. Figure 2 shows these regimes and the respective condensate scaling laws.

$$\alpha_{\text{peak}} = 0, \quad \alpha_{\text{smooth}} = \frac{\beta - \gamma}{2\beta - \gamma}, \quad \alpha_{\text{rect}} = \frac{\beta - \gamma}{\beta - \gamma + 1}. \tag{14}$$

3. Methods

We will employ the empirical method of taking samples while evolving a Markov process. Once we have obtained a set of representative samples for one particular parametrization
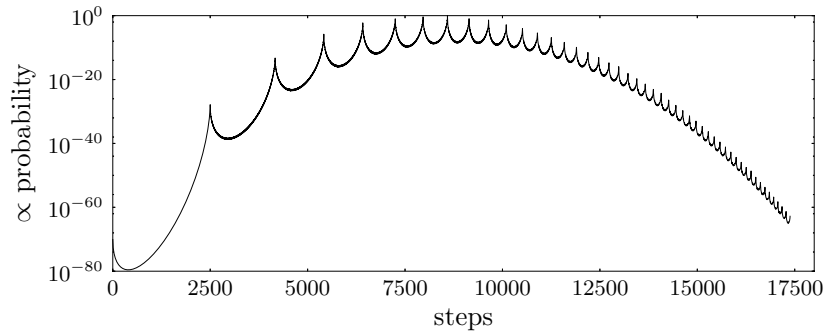
Figure 3. The shortest path in probability landscape starting from a condensate occupying a single site with 5000 particles and going to rectangular condensates of increasing widths. The peaks correspond to the high statistical weights of rectangular condensates and the valleys to those of the transitional states on an ideal trajectory. The (unnormalized) probabilities are based on the parametrization with $\beta = 0.6$, $\gamma = 0.4$.

$(\beta, \gamma, M_\mathrm{c})$, we can determine the condensate width. With the widths for different condensate volumes M_c, we then can estimate the condensate-width scaling exponent α.

3.1. Generating system samples

The straightforward method for generating samples is to simulate the process as defined. Its dynamics with typically small transition probabilities leads to a large waiting time until the gathered samples are representative. The key ingredient for improving the simulation is that one knows the steady state probabilities (1) which are invariant under the employed dynamics, asymmetric hopping ($r \neq 1/2$) in non-equilibrium or symmetric hopping ($r = 1/2$) in equilibrium. In the latter case, we can verify stationary equivalence to systems with other dynamics that yield the same distribution, but mix much more quickly. The Metropolis dynamics is known to mix well and can be readily adjusted for the desired distribution, which is why we chose to use it in our simulations. When the update scheme is altered so that particles may hop to any site instead of just the nearest neighbours, the simulation algorithm assumes the form:

 (i) Select randomly a site from which a move of one particle is attempted.
 (ii) If this site is empty, the system remains in the same state for another time step of $1/N$ sweeps. If it is occupied, choose any of the other sites as a destination site.
(iii) Accept the move with Metropolis probability $P_\mathrm{acc} := \min (P_\mathrm{final}/P_\mathrm{initial}, 1)$ or remain in the current state for another time step otherwise, where P_initial and P_final are the probabilities of the microstates before and after the proposed move, respectively.

For our implementation of the simulation we use the reference implementation of a variant of the Mersenne twister pseudo-random number generator [13, 14].

This approach works well for the smooth condensate shape region ($\beta \geqslant 1$), where the probability landscape is marginally rugged. For systems in the rectangular condensate regime this is not the case anymore because the probability landscape is heavily rugged as shown in figure 3. The transitional states between rectangular condensates of different widths are suppressed by several orders of magnitude and simulations with single-particle (or local) updates mix slowly.

In order to address this issue, we designed an additional set of multi-particle (non-local) updates that allow jumps between high probability regions, which correspond to the peaks in

figure 3, in a single step, thus bypassing the suppressed transitional states. This is achieved by defining a condensate expansion and reduction transformation, where the condensate width is increased or decreased by about one unit.

With the above described local update algorithm it is easy to verify that the resulting stationary distribution is given by equations (1), (3) and (5). By changing the dynamics we must be careful to keep the steady state unchanged. The local update performs well in exploring the landscape locally, which is why we will keep it and independently add non-local updates. The probability currents added by the new updates must cancel each other out in every state. This can be achieved by constructing a dynamics fulfilling detailed balance, where an incoming probability current is being cancelled by the corresponding outgoing one. The one we used before and which we will use again is based on Metropolis transition rates. The main problem here is to treat equally the two non-local update moves and how often to use them in order to minimize the relaxation time. We chose to solve this by restricting the number of new transitions that are permitted at any state to (at most) two; an expansion and a corresponding reduction transition. The new simulation algorithm then consists of a preceding step, where a decision (according to some predefined probability) is made on whether to attempt a local or a non-local step[2]. Choosing a local update is followed by the algorithm above, while a non-local update is governed by the following algorithm:

 (i) Decide whether to attempt an expansion or reduction transformation with equal probability.
 (ii) If the chosen transformation is not valid, the system remains in the current state for another time step (the system is constrained in a similar way to the situation of attempting to move a particle from an unoccupied site), otherwise continue.
(iii) Accept the transformation with Metropolis probability $P_{acc} = \min(P_{final}/P_{initial}, 1)$ or remain in the current state for another time step otherwise.

From the algorithm above, the necessary conditions are that there should be only one way (if any) to expand or reduce the condensate and the transformation must be invertible such that reducing a previously expanded state always results in the original state.

The conditions we decided on is that expansion transformations are eligible only if the original state has two unoccupied sites to the right of the condensate. One removes particles from the top of the condensate by sweeping from left to right and puts them on the empty site right to the condensate, until the two last condensate sites have the same occupation numbers (in some cases this is not possible, then the transformation is invalid). Likewise, reduction transformations are only valid if the original state has the same occupation numbers at the two rightmost condensate sites. One removes the particles at the rightmost condensate site and distributes them by sweeping from left to right onto the rest of the condensate. Figure 4 gives an example of both transformations.

For $M = 1000$ particles with $\beta = 0.7$ and $\gamma = 0.4$ the autocorrelation time of the condensate width of purely local updates is about ten times larger than that of non-local updates. Increasing the particle number by 50% (100%) increases this factor to 50 (250). Whereas the new method enables systems with more than 10^6 particles to mix sufficiently in less than an hour, purely local updates are constrained to less than 10^4 particles.

In cases where β and γ are both close to 0, the critical density is so large, that the condensate is not surrounded by unoccupied sites anymore. Our non-local updates are then rendered ineffective and there is no easy way to adjust them to this situation.

---

[2] For small probabilities it is better to use the waiting time until a non-local update will be performed, which is geometrically distributed.
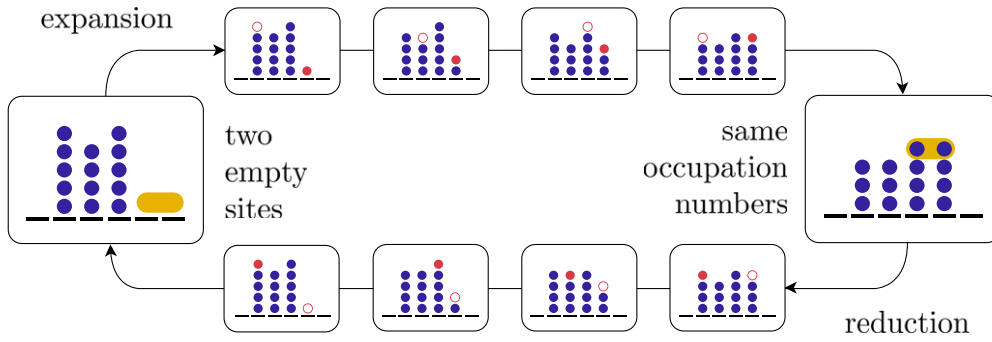
Figure 4. The transformation loop for an example condensate state including all intermediate steps. Any condensate state is suitable for the respective transformation if it fits either starting point in this loop and adheres to the highlighted characteristics.
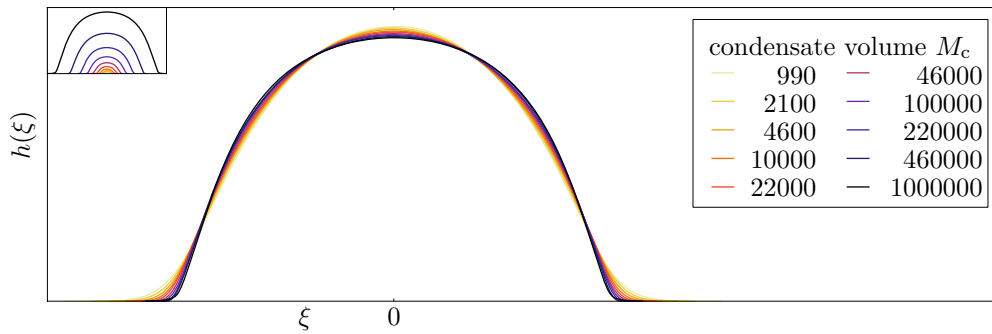

Figure 5. Comparison of mean condensate shapes at different volumes but the same parametrization $\beta = 1.2$ and $\gamma = 0.3$. The shapes were rescaled in terms of extension by the condensate width and in terms of occupation numbers by normalization to a unit volume. With increasing condensate volumes the shapes converge to a single shape which indicates a common *characteristic shape* for this parametrization. The inset shows the original mean condensate shapes.

3.2. Determining the condensate width

In the analytic approximation of the scaling behaviour [12], the width of the condensate is defined as the distance between the two outmost sites of the condensate, which we will call the condensate extension W (see figure 6(a)). Whereas this is a good choice in the thermodynamic limit, for finite systems the condensate edges are subject to interactions with the rest of the system, which results in the edges being smeared outward the condensate. The condensate extension is an observable that is strongly influenced by these finite-size effects, and therefore overestimates the condensate width. This is especially the case with narrow but high condensates that have steep edges.

We decided to measure the condensate width with another observable that is less prone to these smearing-out effects. This observable is based on the assumption that given a parametrization β and γ, the system exhibits a common characteristic shape that is merely rescaled in width and height in dependence on the volume of the condensate. Reversing this assumption, it must be possible to rescale condensate shapes of different volumes to such a common shape, which was done for one example system in figure 5. One can see there, that as
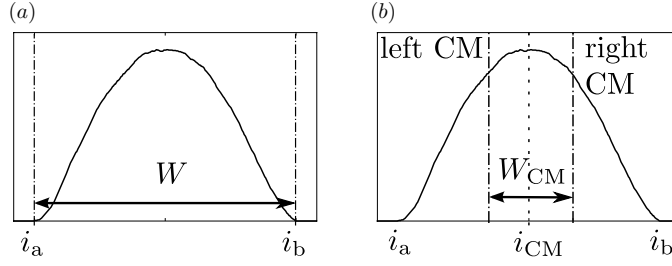
Figure 6. Condensate width determination method by (*a*) taking the direct condensate base extension or (*b*) taking the distance of the left and right condensate wings' respective centres of mass W_{CM}.

condensate volumes increase, the shapes converge to a characteristic shape, with small volume condensates deviating from it due to the mentioned finite-size effects.

First the condensate is separated in two wings left and right of its centre of mass (CM) position $i_{\mathrm{CM}} = \sum_{i=i_a}^{i_b} i m_i / M_{\mathrm{c}}$, where i_a and i_b are the start and end positions of the condensate so that $m_i > 0$ for $i_a < i < i_b$. Then we calculate the width as the distance between the individual CM of these two wings,

$$W_{\mathrm{CM}} = \frac{2}{M_{\mathrm{c}}} \left(\sum_{i \geqslant i_{\mathrm{CM}}}^{i_b} i m_i - \sum_{i_a}^{i < i_{\mathrm{CM}}} i m_i \right). \tag{15}$$

Figure 6 summarizes how this is done in comparison to the direct estimation method.

3.3. Determining the condensate width scaling behaviour

Once we have obtained estimates of the wing CM width observable W_{CM} for system parametrizations with different condensate volumes M_{c}, the prediction [12] states that for large volumes the scaling behaviour adheres to $W_{\mathrm{CM}} \propto M_{\mathrm{c}}^{\alpha}$ with $\alpha(\beta, \gamma)$. Taking the logarithm this relation reduces to a linear relationship with α determining the slope. Figure 7 confirms that the data asymptotically approaches this linear relationship with increasing condensate volumes. Determining the scaling exponent is a linear regression problem, where the measured condensate width is uncertain but the measured condensate volume is considered certain. A minor problem is the overestimation of the condensate width for small condensates with strong smearing (finite-size) effects, which we simply avoid by simulating large enough condensates.

One potentially problematic aspect left untouched so far, is how the condensate width and with it the scaling behaviour is affected by the system size, especially considering effective interactions between the condensate edges through the background. The measurements in figure 8 show that for systems where the condensate volume stays the same, but the system size changes, the measured condensate width remains unchanged as long as $\rho > \rho_c$. This leads to the conclusion that for densities much larger than the critical density, the competition between the gaseous background and condensate phase is dominated by the latter. This system size independence is favourable for us, since it eliminates one degree of freedom in the discussion (leaving only the system parametrization β, γ and condensate volume M_{c}) and allows us to choose systems sizes that are sufficient for the condensates, but small enough to maintain simulation performance. We used a fixed size about ten times the width of the largest condensate to minimize interaction of condensate edges around the boundary and eliminate percolating condensates.
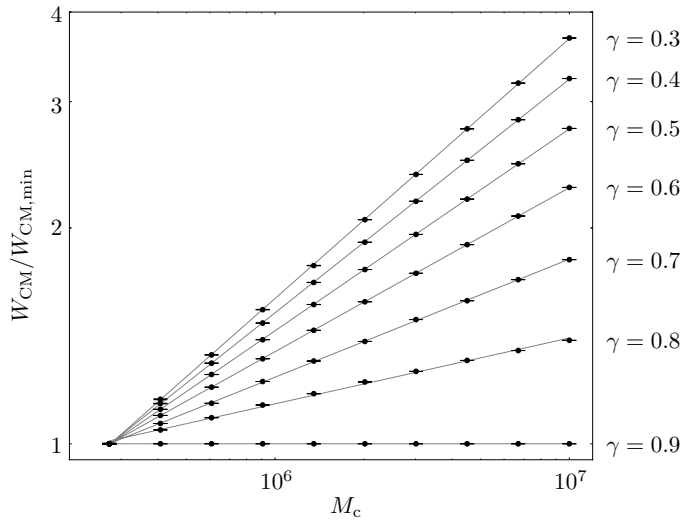
Figure 7. Log–log plot of the width scaling behaviour in dependence on the condensate volume M_c for systems with $\beta = 0.9$ and various γ in the range [0.3, 0.9]. The wing centre-of-mass widths (15) have been normalized by dividing them by the smallest width.
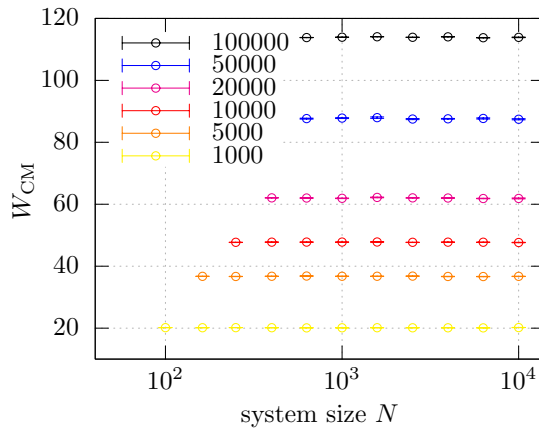
Figure 8. The dependence of the condensate width with a fixed condensate volume M_c on the system size for $\beta = 1.3$ and $\gamma = 0.5$. The critical density is about $\rho_c \simeq 0.14$.

4. Results

We are first going to look at the condensate phases, where especially the boundary between the smooth and rectangular condensate phase is of interest. Then we will present the estimated condensate width scaling behaviour.

4.1. Condensate phases

In order to determine the phases we will use the previously introduced concept of characteristic shapes. Figure 9 shows estimations of these shapes for a range of points in parameter space

Figure 9. Comparison of the characteristic shapes for systems of various β and γ at a condensate volume of about 10^5 masses. 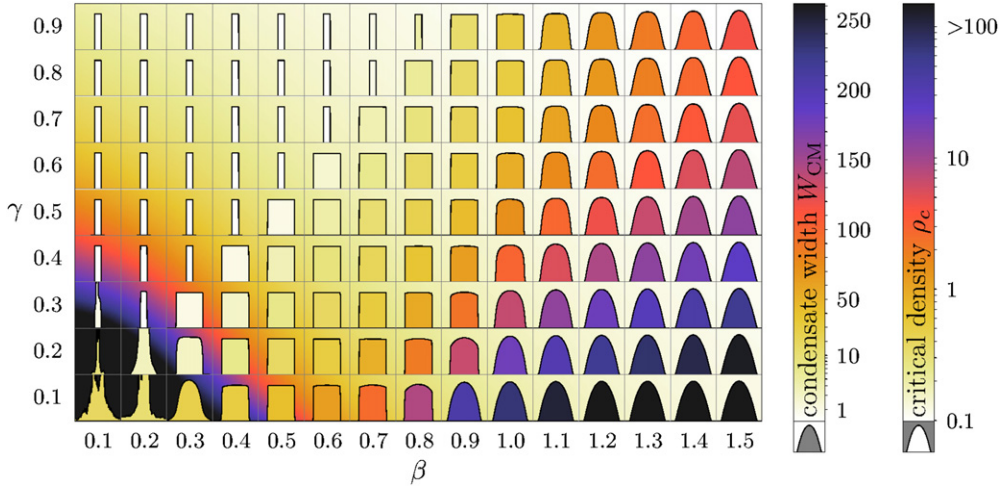The shapes are formed by rescaling the width and height of all measured condensate sample shapes and only then averaging them (this avoids averaging artefacts one would get when interchanging these two steps). The fill colour inside the condensate shapes encodes the respective measured condensate width while the background colour around the shapes gives the critical density of the system. The shapes in the single-site condensate regime are plotted narrowed to give better distinction to extended shapes.

at a system volume of about 10^5 masses. The data is obtained in runs with on the order of 10^8 Monte Carlo sweeps (consisting of N single-particle moves) taking 10^4 samples of the system. For $\beta \lesssim 1$ we see characteristic shapes with constant elevation in the middle section and steep edges at the boundaries, which correspond to the predicted rectangular condensate shape. For small β and γ we see that the estimation of the characteristic shape fails. This is due to the increased critical density and the associated failure of the non-local update. The detection method used here is unable to distinguish between extended rectangular condensates and peak-shaped single-site condensates.

For $\beta \gtrsim 1$ we see characteristic shapes with decreasingly steep edges that converge to a dome. These bell-shaped condensates correspond to the smooth case that was predicted for this region. For small γ and $\beta \approx 1$ the condensation process is close to the purely interaction driven process (4) for which the characteristic shape

$$h(\xi) = \frac{w}{2v} \log\left[\frac{\cosh J - \cosh v\xi}{\cosh J - \cosh v}\right], \quad \text{with} \quad \xi = \frac{2i}{W} - 1, w = 2.2005, v = 0.5413, J = 1$$

(16)

can be analytically approximated [12], as compared in figure 10. The measured shape is similar to this approximation and as β increases, this characteristic shape seems to describe large γ systems as well.

The phase boundary in our measurements is not a clear separation at $\beta = 1$ between the two phases, as the predictions suggest, but it seems to be smeared out in favour of smooth condensates for small γ and in favour of rectangular condensates for large γ. In the respective regions the measured shapes combine characteristics of the individual phases. Once we have steep edges with smooth domes and on the other side we have slowly rising edges with a flat plateau on top. A comparison of the finite-size shapes corresponding to different
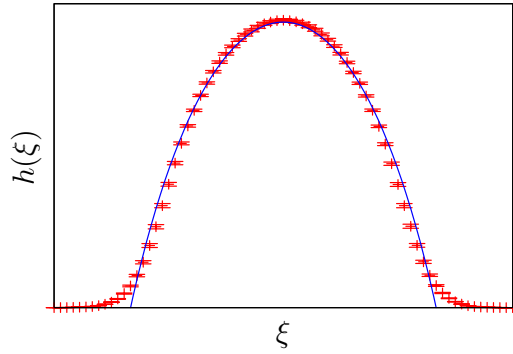
Figure 10. Comparison of the rescaled condensate shape for $\beta = 1, \gamma = 0.2, M = 1000$ with the exact shape (16) derived in [12] (blue line) for the interaction driven process (4).
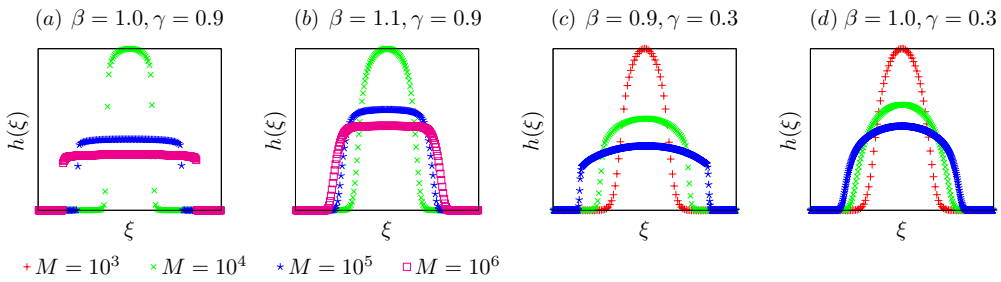

(a) $\beta = 1.0, \gamma = 0.9$ (b) $\beta = 1.1, \gamma = 0.9$ (c) $\beta = 0.9, \gamma = 0.3$ (d) $\beta = 1.0, \gamma = 0.3$

$+ M = 10^3$ $\times M = 10^4$ $\star M = 10^5$ $\square M = 10^6$

Figure 11. Finite-size effects of the condensate shape near the rectangular/smooth transition. The total amounts of masses in the system corresponding to the plotted rescaled shapes have increasing width $M = 10^4$, $M = 10^5$, $M = 10^6$ for $\gamma = 0.9$ and $M = 10^3$, $M = 10^4$, $M = 10^5$ for $\gamma = 0.3$, respectively. For $\beta < 1$, the smooth condensate edges disappear for increasing particle numbers M while they stay for $\beta > 1$.

condensate sizes given in figures 11(a)–(d) indicates that the transition line will sharpen with increasing condensate size, supporting that we are dealing with finite-size effects. However, the prediction only tells us in the leading order which phase dominates for infinitely large condensate volumes, but not whether there is a crossing where both phases are equally likely and at which volume this would occur. Therefore, the deviation of scaling exponents from the prediction could also imply that those systems have higher-order corrections to the transition.

4.2. Condensate width scaling

Figure 12 shows the estimated scaling exponents for the width-scaling behaviour of the smooth and rectangular case, with the measured values listed in table 1. One can see that for $\beta > 1$ the measurements align well with the predictions, except for small γ values, where the deviations can be the result of finite-size effects. There, zero-range interactions are weak and the condensates span many sites, which eventually becomes unfeasible to simulate for large condensate volumes. In the case $\beta < 1$ and large γ, the estimates are very close to the predicted values. Combining the scaling behaviour with the characteristic shapes, we see that for $\beta > 1.5$ the condensate shape and scaling exponent is close to the behaviour of purely interaction-driven condensation, even for γ close to 1.

Table 1. Table of measured values of scaling exponents α (upper values) and their respective absolute deviations from the predicted values (lower values). For the referred theoretical predictions see equation (14). To estimate these scaling exponents we performed on the order of 10^9 Monte Carlo sweeps to take about 10^5 samples.

		γ								
		0.1	0.2	0.3	0.4	0.5	0.6	0.7	0.8	0.9
	0.1	0.00 (10)	0.00 (10)	0.00 (10)	0.00 (10)	0.00 (10)	0.00 (10)	0.00 (10)	0.00 (10)	0.00 (10)
		+.00	+.00	+.00	+.00	+.00	+.00	+.00	+.00	+.00
	0.2	0.05586 (68)	0.00 (10)	0.00 (10)	0.00 (10)	0.00 (10)	0.00 (10)	0.00 (10)	0.00 (10)	0.00 (10)
		−.14677	+.00	+.00	+.00	+.00	+.00	+.00	+.00	+.00
	0.3	0.01809 (98)	0.0389 (33)	0.00 (10)	0.00 (10)	0.00 (1.0)	0.00 (10)	0.00 (10)	0.00 (10)	0.00 (10)
		−.14857	−.0520	+.00	+.00	+.00	+.00	+.00	+.00	+.00
	0.4	0.1551 (67)	0.13103 (78)	0.06497 (12)	0.00 (10)	0.00 (10)	0.00 (10)	0.00 (10)	0.00 (10)	0.00 (10)
		−.0757	−.03564	−.02594	+.00	+.00	+.00	+.00	+.00	+.00
	0.5	0.2260 (18)	0.2017 (11)	0.15376 (32)	0.079277 (96)	0.00 (10)	0.00 (10)	0.00 (10)	0.00 (10)	0.00 (10)
		−.0597	−.0291	−.01291	−.011632	+.00	+.00	+.00	+.00	+.00
	0.6	0.2927 (11)	0.26195 (75)	0.21893 (29)	0.16164 (12)	0.087798 (21)	0.00 (10)	0.00 (10)	0.00 (10)	0.00 (10)
		−.0407	−.02376	−.01184	−.00503	−.003111	+.00	+.00	+.00	+.00
	0.7	0.34117 (87)	0.31238 (27)	0.27406 (27)	0.22512 (11)	0.165949 (43)	0.089215 (94)	0.00 (10)	0.00 (10)	0.00 (10)
		−.03383	−.02096	−.01166	−.00565	−.000718	−.001694	+.00	+.00	+.00
	0.8	0.38282 (67)	0.35627 (38)	0.32126 (31)	0.27958 (12)	0.227928 (52)	0.168049 (28)	0.097067 (61)	0.00 (10)	0.00 (10)
		−.02895	−.01873	−.01208	−.00613	−.002841	+.001382	+.006158	+.00	+.00
	0.9	0.4623 (10)	0.39033 (47)	0.36312 (34)	0.32649 (18)	0.282072 (77)	0.229113 (33)	0.163916 (12)	0.081862 (50)	0.00 (10)
		+.0178	−.02143	−.01188	−.00684	−.003642	−.001656	.002750	−.009047	+.00
β	1.0	0.46611 (67)	0.43925 (58)	0.40296 (51)	0.36059 (46)	0.32191 (51)	0.27902 (31)	0.229285 (63)	0.165404 (20)	0.08919 (11)
		−.00758	−.00520	−.00880	−.01441	−.01142	−.00670	−.001484	−.001262	−.00172
	1.1	0 47105 (59)	0.44486 (49)	0.41672 (43)	0.38415 (37)	0.34759 (32)	0.30853 (27)	0.26286 (22)	0.21143 (18)	0.15211 (17)
		−.00514	−.00514	−.00433	−.00474	−.00535	−.00397	−.00381	−.00285	−.00173
	1.2	0.47340 (57)	0.45060 (46)	0.42709 (37)	0.39673 (31)	0.36528 (35)	0.33210 (35)	0.29166 (32)	0.24856 (31)	0.19675 (27)
		−.00487	−.00394	−.00148	−.00327	−.00314	−.00123	−.00245	−.00144	−.00325
	1.3	0.47459 (55)	0.45386 (44)	0.43267 (36)	0.40755 (27)	0.37863 (24)	0.34801 (20)	0.31296 (22)	0.27588 (20)	0.23271 (18)
		−.00541	−.00448	−.00211	−.00154	−.00232	−.00199	−.00283	−.00190	−.00258

Table 1. (Continued.)

|					γ				
	0.1	0.2	0.3	0.4	0.5	0.6	0.7	0.8	0.9
1.4	0.47652 (50)	0.45820 (39)	0.43626 (35)	0.41410 (25)	0.38885 (22)	0.36133 (18)	0.33114 (13)	0.29712 (12)	0.26078 (12)
	−.00497	−.00334	−.00374	−.00257	−.00245	−.00231	−.00219	−.00288	−.00237
1.5	0.47755 (48)	0.45842 (39)	0.44011 (33)	0.41960 (25)	0.39772 (19)	0.37261 (17)	0.34580 (12)	0.316235 (100)	0.28340 (11)
	−.00521	−.00586	−.00433	−.00348	−.00228	−.00239	−.00203	−.001947	−.00231
1.6	0.47679 (44)	0.45910 (36)	0.44299 (31)	0.42405 (23)	0.40435 (19)	0.38183 (16)	0.35761 (12)	0.33100 (10)	0.30196 (11)
	−.00708	−.00757	−.00529	−.00453	−.00306	−.00278	−.00239	−.00233	−.00239
1.7	0.47782 (46)	0.46184 (35)	0.44528 (29)	0.42823 (22)	0.40938 (19)	0.38965 (13)	0.36778 (12)	0.344148 (95)	0.31735 (11)
	−.00703	−.00691	−.00633	−.00510	−.00441	−.00321	−.00260	−.002006	−.00265
1.8	0.47948 (46)	0.46234 (35)	0.44750 (25)	0.43121 (23)	0.41431 (18)	0.39633 (13)	0.37680 (10)	0.354548 (98)	0.33038 (10)
	−.00624	−.00824	− .00705	−.00629	−.00504	−.00367	−.00251	−.002594	− .00295
1.9	0.47933 (45)	0.46190 (34)	0.44962 (27)	0.43441 (22)	0.41868 (18)	0.40221 (12)	0.38326 (12)	0.363798 (92)	0.341784 (99)
	−.00716	−.01032	−.00753	−.00677	−.00556	−.00404	−.00383	−.002868	−.003044
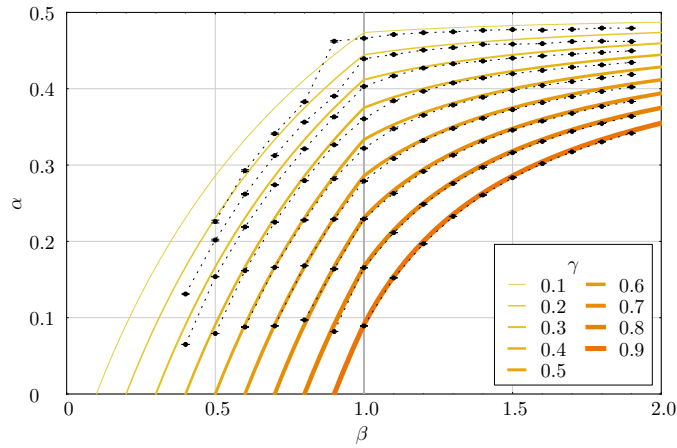
Figure 12. The measured scaling behaviour in the rectangular and smooth phases as a function of β. In contrast to the phase diagram in figure 2, the scaling exponent α is not shown in a 'depth' dimension, but as the y-value. Points for the same value of γ are connected by broken lines. The continuous coloured lines correspond to the predicted values for the scaling exponent α given by equation (14). The underlying condensate volumes are in the range of 3×10^3 to 10^7, depending on how extended the condensates and therefore how computationally expensive the simulations are.

One region where the measurements deviate strongly from the predictions is for small γ in the rectangular case. This region is also where the scaling behaviour is predicted to change dramatically at the phase boundary. It looks like the measurements of scaling exponents change in the same way as the predictions, but shifted to lower values. We have found no explanation so far why these systems behave this way. The obvious measurement outlier at position $\beta = 0.9$ and $\gamma = 0.1$ can however be explained as an extension of the smooth scaling behaviour, which agrees with the observation that the condensate shape has no rectangular characteristics.

The region at $\beta = 1$ is of special interest, as there the condensate not only gradually changes from a smooth to a rectangular shape as γ grows from 0 to 1, but covers the whole scaling exponent range from 0 to 0.5 as well. In this region it also becomes feasible to simulate the original dynamics and thus investigate dynamical properties of these systems as well.

The peak condensate region $\beta < 1$, $\gamma > \beta$, with the transition line $\beta = \gamma$ is reproduced sufficiently well with problems at small values of γ due to exceedingly large critical density as visible in the background colour code in figure 9. Here we observe zero-range process like condensates as the local interaction term is strongly dominant.

5. Summary

Based on the improved simulation method, especially in the rectangular phase, we were able to show for the pair-factorized steady state model (5) that the three phases predicted in [11, 12] with peak-like, rectangular and smooth (bell-like) condensate shapes exist in about the regions they are expected in. By analysing the characteristic shapes, we found that the finite systems we considered exhibit finite-size effects that smear out the phase boundary between rectangular and smooth, bell-like shaped condensates.

With the improved estimator for the condensate scaling behaviour we were able to confirm that the scaling behaviour is clearly different from that of purely interaction-driven condensation processes [10]. Table 1 demonstrates that the estimates for large regions of the

parameter space are close to the expected scaling behaviour. In the smooth phase, the measured scaling exponents are within 2% of the analytically predicted values, which verifies that the assumptions and approximations in the analytical predictions of [12] are justified. In fact, the prediction yields very good values of the scaling exponents even for finite systems provided no transition line is close. Systematic deviations of the transition line between the rectangular and smooth condensate shape regimes that we observed are largely due to finite-size effects.

Acknowledgments

References

[1] Derrida B, Domany E and Mukamel D 1992 *J. Stat. Phys.* **69** 667–87
[2] Schütz G and Domany E 1993 *J. Stat. Phys.* **72** 277–96
[3] Spitzer F 1970 *Adv. Math.* **5** 246–90
[4] Chowdhury D, Schadschneider A and Nishinari K 2005 *Phys. Life Rev.* **2** 318–52
[5] Chowdhury D, Santen L and Schadschneider A 2000 *Phys. Rep.* A **329** 199–329
[6] Evans M R 2000 *Braz. J. Phys.* **30** 42–57
[7] Evans M R, Foster D P, Godrèche C and Mukamel D 1995 *Phys. Rev. Lett.* **74** 208–11
[8] Evans M R and Hanney T 2005 *J. Phys. A: Math. Gen.* **38** R195–240
[9] Majumdar S N 2010 *Exact Methods in Low-Dimensional Statistical Physics and Quantum Computing* (*Les Houches Lecture Notes Summer School* vol 89) ed J Jacobsen, S Ouvry, V Pasquier, D Serban and L F Cugliandolo (Oxford: Oxford University Press) pp 407–30
[10] Evans M R, Hanney T and Majumdar S N 2006 *Phys. Rev. Lett.* **97** 010602
[11] Wacław B, Sopik J, Janke W and Meyer-Ortmanns H 2009 *Phys. Rev. Lett.* **103** 080602
[12] Wacław B, Sopik J, Janke W and Meyer-Ortmanns H 2009 *J. Stat. Mech.* P10021
[13] Matsumoto M and Nishimura T 1998 *ACM Trans. Model. Comput. Simul.* **8** 3–30
[14] Saito M and Matsumoto M 2009 *Monte Carlo and Quasi-Monte Carlo Methods 2008* ed P L'Ecuyer and A B Owen (Berlin: Springer) pp 589–602